agronomy

MDPI

Article

Divergent Strategies Within a Shared Functional Framework Drive Niche Differentiation of Dominant Halophytes Along a Salinity–Alkalinity Gradient

Shaojuan Mao [1,2], Zengbi Yue [3], Yang Wu [4], Meng Liang [1,4], Haoxiang Xue [1,4], Fawei Zhang [5], Guobin Liu [4] and Sha Xue [1,4,*]

[1] State Key Laboratory of Soil and Water Conservation and Desertification Control, College of Soil and Water Conservation Science and Engineering, Northwest A&F University, Yangling 712100, China; sj.mao@qhu.edu.cn (S.M.); lemon960512@163.com (M.L.); xhx3409039852@163.com (H.X.)
[2] College of Ecological and Environmental Engineering, Qinghai University, Xining 810016, China
[3] Power China Northwest Engineering Corporation Limited, Xi'an 710065, China; xby02157@powerchina.cn
[4] Institute of Soil and Water Conservation, Chinese Academy of Sciences, Yangling 712100, China; wuyang0521@nwsuaf.edu.cn (Y.W.); gbliu@ms.iswc.ac.cn (G.L.)
[5] Northwest Institute of Plateau Biology, Chinese Academy of Sciences, Xining 810008, China; mywing963@126.com
* Correspondence: xuesha100@163.com

Abstract

How functional trait responses relate to niche differentiation among dominant halophytes along multidimensional environmental gradients remains unclear. This study investigated three co-dominant halophyte species in two representative saline–alkali habitats in northwestern China. We quantified niche differentiation and trait responses along gradients of soil salt content (SSC) and sodium adsorption ratio (SAR) and compared stress–trait–performance relationships among species. The three species differed in niche position within the SSC-SAR space, with overlapping niche distributions. *Nitraria tangutorum* Bobrov occupied habitats characterized by high SAR and low SSC, *Salicornia europaea* L. was associated with high SSC and low SAR conditions, and *Kalidium foliatum* (Pall.) Moq. occupied intermediate environments. Trait responses to SSC and SAR varied among species. *N. tangutorum* showed a negative association between acid detergent fiber (ADF) and biomass, consistent with a structure–growth trade-off, *S. europaea* showed strong coordination between osmotic regulation and nutrient traits, and *K. foliatum* exhibited relatively balanced trait coordination. Multi-group structural equation modeling identified three pathways with significant differences among species after correction for multiple testing. Overall, these findings suggest that niche differentiation among dominant halophytes is associated with variation in trait responses and selected trait relationships along SSC and SAR gradients.

Keywords: saline–alkali land; halophytes; niche differentiation; functional traits; trait coordination; stress–trait–performance relationships

Check for updates

Academic Editor: Fernando França da Cunha

Received: 29 August 2026
Revised: 11 October 2026
Accepted: 13 October 2026
Published: 26 October 2026

Copyright: © 2026 by the authors. Licensee MDPI, Basel, Switzerland. This article is an open access article distributed under the terms and conditions of the Creative Commons Attribution (CC BY) license.

1. Introduction

Saline–alkali land constitutes a vital reserve land resource, covering approximately 6% of the Earth's terrestrial surface [1]. These lands are mainly distributed in arid, semi-arid, and coastal regions. The accumulation of soluble salts profoundly alters soil physical,

chemical, and biological properties, thereby imposing multiple constraints on plant establishment, growth, and reproduction [2,3]. Consequently, patterns of species differentiation and coexistence in saline–alkali ecosystems arise from plant responses to multiple environmental filters. However, these processes are often evaluated using a single salinity-related indicator, which may be insufficient to reveal the underlying mechanisms.

Salinization and alkalization frequently occur concurrently during soil degradation processes [4], yet they impose distinct ecological constraints and elicit different plant responses [5,6]. FAO's Global Map of Salt-Affected Soils classifies 5% of mapped salt-affected topsoils (0–30 cm) and 14% of mapped salt-affected subsoils (30–100 cm) as saline–sodic, illustrating the co-occurrence of salinity and sodicity [7]. Soil salt content (SSC) primarily reflects the degree of salt accumulation and associated osmotic stress [6]. The sodium adsorption ratio (SAR) expresses the relative abundance of Na^+ compared with Ca^{2+} and Mg^{2+} in soil solution and is used to assess sodicity hazard [4]. Pätsch et al. [5] found that species-specific responses to soil ion concentrations did not necessarily correspond to overall salinity or alkalinity, supporting the consideration of ionic composition alongside total salt content. Therefore, plant community differentiation in saline–alkali environments should not be viewed solely as a response to a unidimensional gradient of increasing stress intensity. Rather, species are expected to partition niches and coexist within a multidimensional stress space.

Plant functional traits represent key adaptive attributes that mediate species responses to environmental stress [8,9]. Environmental adaptation is rarely achieved through independent variation in individual traits; instead, it emerges from coordinated shifts, trade-offs, and integration among multiple traits [10,11]. Consequently, niche differentiation may reflect not only differences in environmental occupancy but also divergence in trait coordination strategies [12,13]. However, the links among niche differentiation, trait coordination, and adaptive strategies in saline–alkali ecosystems remain poorly quantified.

Furthermore, the adaptation of different halophytes to saline–alkali environments may reflect either convergent responses to common environmental filters or divergent strategies associated with different dimensions of environmental stress. Functional traits and their plasticity can facilitate species coexistence by mediating ecological differentiation and competitive trade-offs [14]. The long-term persistence of dominant halophytes in high salinity–alkalinity conditions implies that these species share a fundamental adaptive basis for coping with salinity–alkalinity stress. However, differences in habitat occupancy and trait responses indicate that species may achieve successful adaptation through distinct ecological strategies. This raises a key ecological question: to what extent do stress–trait–performance relationships differ among dominant halophytes? Existing trait-based studies have largely examined species distributions [5], trait means [15], trait correlations [9], or individual stress-response pathways [16] in isolation. However, it lacks an integrative framework that links these multiple levels of organization to distinguish convergent adaptation from divergent adaptation and to elucidate the mechanisms underpinning species coexistence in saline–alkali ecosystems.

This study investigated three dominant halophyte species—*Salicornia europaea* L. (hereafter *S. europaea*), *Kalidium foliatum* (Pall.) Moq. (hereafter *K. foliatum*), and *Nitraria tangutorum* Bobrov (hereafter *N. tangutorum*)—in representative saline–alkali habitats of northwestern China. These species were selected as focal dominant halophytes based on their importance values and distributions recorded in community surveys at the two study sites. A dual-stress framework based on soil salt content (SSC) and sodium adsorption ratio (SAR) was employed to quantify niche differentiation, key functional trait responses, and commonalities and differences in stress–trait–performance relationships. The following hypotheses were proposed: (1) the three species would exhibit significant niche differentia-

tion along the dual-stress gradients, accompanied by distinct patterns of trait responses and coordination; and (2) interspecific differences in stress–trait–performance relationships would be concentrated in a limited subset of pathways rather than distributed across the entire pathway network.

2. Materials and Methods

2.1. Study Area and Field Sampling

This study was conducted in two representative saline–alkali habitats in northwestern China: (1) an extremely arid desert saline–alkali zone along the shore of Chaka Lake, Qinghai Province (hereafter Chaka site) and (2) a semi-arid, semi-desert saline–alkali zone along the shore of Huamachi Salt Lake, Dingbian County, Shaanxi Province (hereafter Dingbian site). The Chaka site, located in the eastern Qaidam Basin, represents a typical alpine saline–alkali ecosystem. It is characterized by a mean annual temperature of 2.8 °C and a mean annual precipitation of 224 mm. Vegetation is dominated by alpine steppe and montane desert steppe communities. The Dingbian site is situated in a lacustrine depression within a closed basin at the transition between the Loess Plateau and the Mu Us Sandy Land. It represents a typical temperate desert-steppe saline–alkali ecosystem, with a mean annual temperature of 7.9 °C and a mean annual precipitation of 316 mm.

Field surveys and sampling were conducted in July and August 2021. At the Chaka site, eight transects were established at 100 m intervals. Along each transect, nine 10 × 10 m sampling plots were positioned along a lakeshore-to-upland gradient using a non-equidistant design (50, 50, 100, 100, 100, 200, 300, and 500 m) to capture the full extent of the salinity–alkalinity gradient. At the Dingbian site, eight transects were similarly established at intervals of 100 m. Given the smaller spatial extent of the site, eight 10 × 10 m sampling plots were arranged at uniform 50 m intervals along each transect.

2.2. Soil and Plant Trait Measurements

At each sampling point, a 10 × 10 m plot contained three 2 × 2 m quadrats for community surveys. A total of 72 sampling points were established at the Chaka site and 64 at the Dingbian site. At each sampling point, three quadrats were randomly located, resulting in 216 and 192 quadrats at the Chaka and Dingbian sites, respectively. In each quadrat, community composition, plant height, and vegetation cover of dominant halophytes were recorded. Species importance values (IVs) were calculated separately for each quadrat and then averaged across the three quadrats within each plot to obtain plot-level IVs. For chemical trait measurements, 3–5 individuals of each target species present were randomly selected within each plot. When fewer than three individuals were available, all available individuals were sampled. Above- and belowground material from the sampled individuals was pooled to form one composite sample per species per plot.

Soil samples were collected within each 10 × 10 m point. Five soil cores from the 0–10 cm layer were taken following an S-shaped sampling scheme and pooled to form a composite sample. The resulting plot-level composite soil sample was used to determine soil salt content (SSC) and sodium adsorption ratio (SAR). SAR reflects the relative dominance of Na^+ over Ca^{2+} and Mg^{2+} in the soil solution. Soil samples were extracted using deionized water at a soil-to-water ratio of 1:5. Then, soluble cation concentrations were measured in the filtrate, and SSC was determined using the residue drying-gravimetric method. SAR was calculated as follows:

$$\mathrm{SAR} = \frac{\left[\mathrm{Na}^{+}\right]}{\sqrt{\left(\left[\mathrm{Ca}^{2+}\right] + \left[\mathrm{Mg}^{2+}\right]\right)/2}}$$

where [Na^+], [$Ca2^+$], and [Mg^{2+}] are expressed in mEq L^{-1}. Conversion from mass concentration to equivalent concentration accounted for ion molar mass, valence, and the extraction ratio, and the soil-water extraction ratio (1 g soil to 5 mL extract). The resulting conversion factors were 8.709 mEq L^{-1} per mg g^{-1} for Na^+, 9.975 mEq L^{-1} per mg g^{-1} for Ca^{2+}, and 16.456 mEq L^{-1} per mg g^{-1} for Mg^{2+}. SAR was used as an indicator of soil sodicity.

Five traits were selected to characterize biomass accumulation, nutrient status, structural investment, and soluble carbohydrate status in the dominant halophytes: biomass, total nitrogen (TN), total phosphorus (TP), acid detergent fiber (ADF), and soluble sugars (ss). After H_2SO_4-H_2O_2 digestion, TN and TP were determined using the Kjeldahl method and the molybdenum-antimony colorimetric method, respectively. ADF was determined using the Van Soest method. Soluble sugars were determined using the anthrone colorimetric method. Sampling effort and the number of available core trait observations by species and site are summarized in Table S1.

Biomass of the target species was estimated by integrating the harvest method for herbaceous species with the standard-plant method for shrubs and semi-shrubs. For target individuals within each quadrat, maximum crown length, minimum crown width, and maximum plant height were recorded. The product of crown dimensions and plant height was used as the predictor variable to establish biomass regression models for the three halophytes. At each site, 15 individuals spanning different sizes were sampled for each target species, and all 15 individuals were used to fit the corresponding biomass regression model. The fitted equations and goodness-of-fit statistics are presented in Figure S1. For each target species, biomass was expressed per unit area and averaged across the three quadrats within each plot. Quadrats in which the species was absent were assigned a biomass of zero and included in the calculation.

2.3. Statistical Analysis

Analyses were conducted at the sampling-point (plot) level; quadrats and pooled individuals were subsamples rather than separate analytical replicates. Statistical analyses were performed using R (version 4.5.2). To characterize niche patterns of the three halophytes within the two-dimensional SSC-SAR stress space, generalized additive models (GAMs) were fitted with species importance value (IV) as the response variable, SSC and SAR as explanatory variables, and region as a random effect. The hypervolume method was employed to estimate the niche centroid, niche breadth, and interspecific niche overlap based on the Jaccard and Sørensen indices. GAMs were further fitted to assess the responses of functional traits along SSC and SAR gradients. Five key traits were retained for analysis, including biomass, TN, TP, ss, and ADF. These indicators represent plant size, nutritional status, osmotic adjustment, and structural stress resistance, respectively. GAM convergence, residual patterns, and basis-dimension adequacy were checked. Effective degrees of freedom (edf) characterized the complexity of the penalized SSC–SAR response surface. Hypervolume sensitivity to bandwidth and environmental-variable transformation was assessed using direct importance-value weighting.

To examine trait coordination and trade-offs, sparse partial correlation networks were constructed using EBICglasso based on standardized residuals after accounting for the shared effects of SSC and SAR. The network structure was characterized by edge sign and weight, as well as node strength and expected influence. Finally, species-specific SEMs were developed. Biomass was used as the ultimate response variable; ss, ADF, and a composite nutrient index derived from TN and TP were adopted as mediating traits; and SSC, SAR, their interaction, and region were used as covariates. Multi-group structural equation modeling (MG-SEM) was subsequently applied to compare unconstrained and

equality-constrained models. Region was included as a fixed effect in species-specific SEMs but not in MG-SEM; neither SEM framework explicitly modeled transect-level dependence. Shared and species-specific pathways were identified through nested model comparisons with sequential release of equality constraints. To control for the false discovery rate arising from multiple testing, *p*-values were adjusted using the Benjamini–Hochberg procedure.

3. Results

3.1. Co-Occurring Species Occupied Distinct Positions in the SSC-SAR Stress Space

GAM analyses revealed that all three halophytes exhibited significant nonlinear responses to combined salinity–alkalinity stress ($p < 0.001$), with pronounced interspecific differences in response surface complexity. The response surface of *S. europaea* (edf = 11.17) and *K. foliatum* (edf = 9.37) was more complex than that of *N. tangutorum* (edf = 4.17) (Figure 1). The proportion of deviance explained by salinity–alkalinity stress was higher for *S. europaea* (deviance explained = 45.0%) and *K. foliatum* (40.9%) than for *N. tangutorum* (15.9%). PIV response surfaces indicated species-specific differences in environmental response patterns. *S. europaea* exhibited a broad high-PIV region concentrated under high SSC and moderate-to-low SAR conditions, whereas *N. tangutorum* was associated with low SSC and high SAR environments. *K. foliatum* occupied an intermediate position. High-PIV regions overlapped, but predicted response peaks occurred at different SSC–SAR combinations.

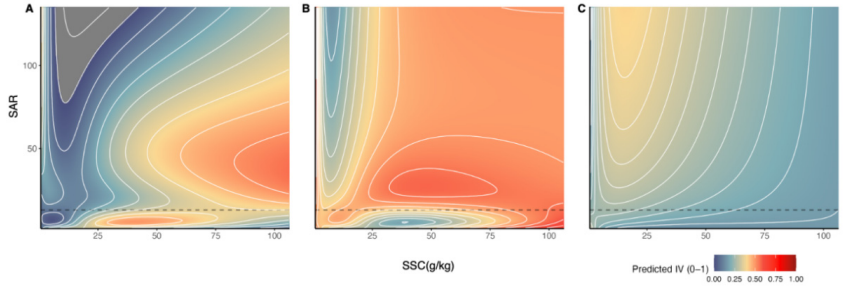


Figure 1. Species-specific niche response surfaces across the SSC-SAR stress space. GAM-predicted importance values are shown for *S. europaea* (**A**), *K. foliatum* (**B**), and *N. tangutorum* (**C**). Warmer colors denote higher predicted importance values, while white contour lines represent equal-response isolines. The three species exhibited distinct high-response zones within the two-dimensional salinity–sodicity space.

PIV-weighted hypervolume analysis (Table 1) further supported this pattern. The niche centroid of *S. europaea* was positioned in high-SSC, low-SAR environments; *K. foliatum* occupied intermediate conditions; and *N. tangutorum* was shifted toward low-SSC, high-SAR habitats. Interspecific niche overlap was relatively high, with Jaccard indices ranging from 0.61 to 0.71 and Sørensen indices from 0.76 to 0.83. Among species pairs, niche overlap was greatest between *S. europaea* and *K. foliatum* and lowest between *S. europaea* and *N. tangutorum*. These patterns indicate differences in environmental positioning within broadly overlapping niches, rather than strong niche segregation.

Table 1. Two-dimensional niche characteristics and pairwise overlap among the three halophytes.

Species-level niche metrics			
Species	**Niche Centroid (SSC, g kg^{-1})**	**Niche Centroid (SAR)**	**Niche Breadth (RMS Distance, log1p Space)**
S. europaea	33.44	12.16	0.95
K. foliatum	28.83	14.23	1.09
N. tangutorum	20.40	17.68	1.17

Table 1. *Cont.*

Pairwise niche overlap		
Species Pair	**Jaccard Similarity**	**Sørensen Similarity**
S. europaea × *K. foliatum*	0.71	0.83
S. europaea × *N. tangutorum*	0.61	0.76
K. foliatum × *N. tangutorum*	0.66	0.79

Niche centroids are presented on the original SSC and SAR scales for interpretability, although hypervolumes were estimated in log1p-transformed SSC-SAR space. Niche breadth was calculated as the weighted root-mean-square distance from the niche centroid in log1p-transformed SSC–SAR space and is reported on this transformed scale, without physical units.

3.2. Key Traits Exhibited Species-Specific Response Surfaces to Dual Stress

The responses of key traits (biomass, TN, TP, ADF, and ss) to SSC and SAR gradients were species-specific (Figure 2 and Table S3). Standard errors and 95% simulation intervals for ΔE are provided in Table S4. Along the SAR gradient, biomass ΔE was negative for *K. foliatum* and *S. europaea* (−142.88 and −456.68, respectively) but positive for *N. tangutorum* (90.32); only *S. europaea* had a 95% simulation interval excluding zero. Along the SSC gradient, *K. foliatum* and *S. europaea* displayed marked increases at SSC ≈ 6.80 (ΔE ≈ +815.81 and +429.10, respectively), whereas *N. tangutorum* showed only a weak response at SSC ≈ 13.52 (ΔE ≈ −11.39).

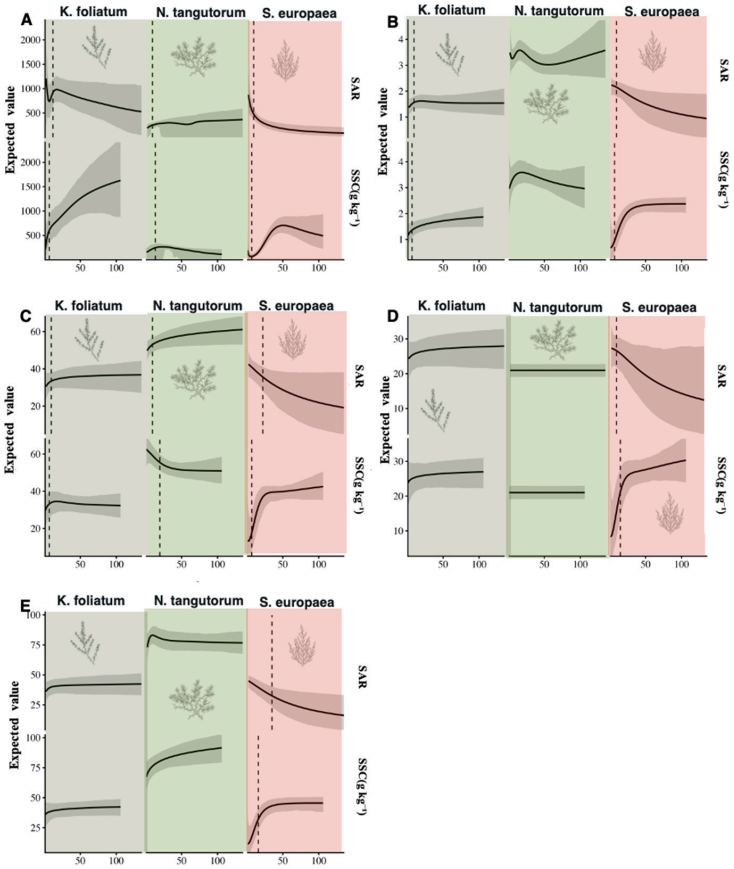


Figure 2. Species-specific 1D trait responses along the SSC–SAR gradient. (**A**) Biomass, (**B**) total phosphorus (TP), (**C**) total nitrogen (TN), (**D**) acid detergent fiber (ADF), and (**E**) soluble sugars (ss). SSC and SAR denote soil salt content and sodium adsorption ratio, respectively. Columns represent species; upper/lower rows show SAR/SSC responses, with the other variable held at its median. Hurdle GAMs combined a binomial model of positive-value probability with a Gamma model of positive values. Solid lines show their combined expected response (probability × conditional positive mean), shaded bands indicate 95% simulation intervals, and dashed lines mark estimated thresholds.

For nutrient traits (TN and TP), along the SAR gradient, TN ΔE was positive for *K. foliatum* and *N. tangutorum* (3.81 and 6.89, respectively) but negative for *S. europaea* (−13.78); the 95% simulation interval included zero only for *K. foliatum*. Along the SSC gradient, TN increased in *S. europaea* at SSC ≈ 6.80 (ΔE ≈ +24.06) but decreased in *N. tangutorum* at SSC ≈ 19.75 (ΔE ≈ −7.19). For TP, *S. europaea* showed a positive response at SSC ≈ 6.80 (ΔE ≈ +1.41) and a negative response at SAR ≈ 9.53 (ΔE ≈ −0.82), whereas no significant threshold response was detected in *N. tangutorum*.

For structural and osmotic regulation traits (ADF and ss), In *S. europaea*, ΔE was positive along SSC and negative along SAR for both ADF (13.88 and −9.27, respectively) and ss (23.24 and −16.23, respectively); only the ADF–SAR interval included zero. No consistent threshold responses in these traits were detected for *K. foliatum* or *N. tangutorum*.

3.3. Functional Trait Coordination Differed Among Species

Environment-adjusted functional trait residual network analysis (Figure 3) revealed clear interspecific differences in network complexity. In the EBICglasso network ($\gamma = 0.20$), only one non-zero partial correlation edge was detected for *K. foliatum* (TP-ss, $\rho = 0.21$; mean absolute partial correlation coefficient $\langle |\rho| \rangle = 0.21$). For *N. tangutorum*, two non-zero edges were detected ($\langle |\rho| \rangle = 0.19$), including TP-ss ($\rho = 0.25$) and ADF-ss ($\rho = 0.12$). In contrast, *S. europaea* exhibited a more complex network with five non-zero edges ($\langle |\rho| \rangle = 0.18$), including positive associations among Biomass-TP ($\rho = 0.30$), TN-TP ($\rho = 0.22$), TP-ss ($\rho = 0.15$), and TN-ss ($\rho = 0.07$), and a negative association between biomass and TN ($\rho = -0.15$). Sensitivity analysis using $\gamma = 0.10$ yielded a consistent network topology (Figure S2 and Table S6).

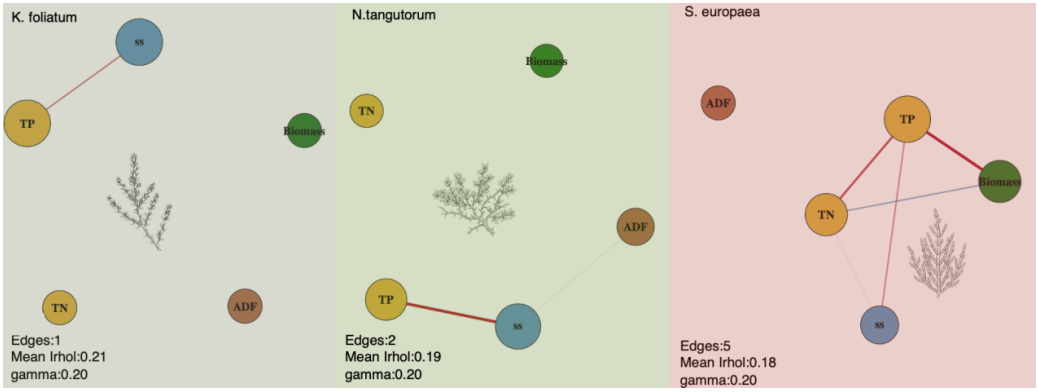


Figure 3. Species-specific functional trait networks of three dominant halophytes. Networks were estimated using EBICglasso ($\gamma = 0.20$) based on environment-adjusted trait residuals from sampling points with complete data for all required variables (*K. foliatum*, $n = 91$; *N. tangutorum*, $n = 122$; *S. europaea*, $n = 106$; both sites combined). Edges represent non-zero partial correlations; red and blue denote positive and negative associations, respectively. Edge width reflects association strength, and node size represents trait strength.

Node centrality analysis (Table S5) indicated that TP was the most influential trait in *S. europaea* (node strength = 0.67), followed by biomass (0.45) and TN (0.45). By contrast, *K. foliatum* and *N. tangutorum* showed lower overall connectivity, with node strength concentrated in the limited number of traits involved in non-zero edges.

3.4. Species-Specific SEMs Revealed Distinct Stress–Trait–Biomass Pathways

Single-species SEMs were fitted using complete sampling-point records from both study sites (*K. foliatum*, n = 91; *N. tangutorum*, n = 122; *S. europaea*, n = 106). The fitted models showed species-specific patterns of association among environmental stress, functional traits, and biomass (Figure 4). In *K. foliatum*, soluble sugars (SS) strongly influenced nutrient

traits (TN and TP) and ADF (β = 0.95 and 0.92, $p < 0.001$). The interaction between SSC and SAR had a negative effect on nutrient traits (β = −0.12, $p < 0.01$). SSC and the SSC × SAR interaction were positively associated with biomass (β = 0.31 and 0.24, respectively). The model explained most variation in nutrient traits and ADF (R^2 = 0.90 and 0.83, respectively) but less in biomass and ss (R^2 = 0.26 and 0.09, respectively).

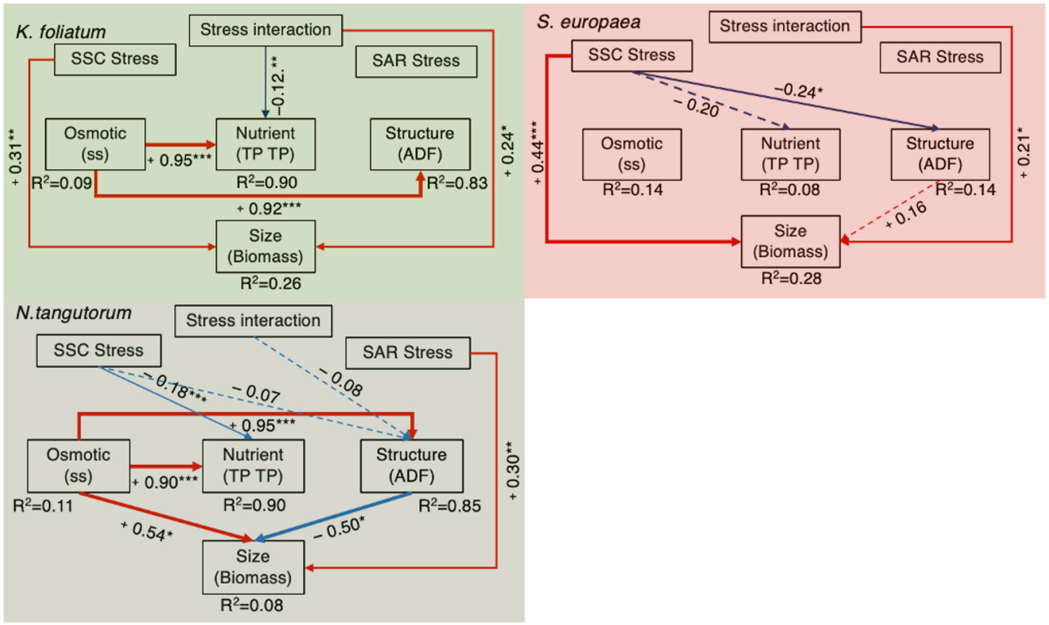


Figure 4. Species-specific structural equation models linking salt–alkali stress, trait coordination, and biomass in three dominant halophytes. Path diagrams are shown for *K. foliatum* (*n* = 91), *N. tangutorum* (*n* = 122), and *S. europaea* (*n* = 106). Numbers on arrows indicate standardized path coefficients. Red and blue arrows denote positive and negative effects, respectively; dashed arrows indicate marginally significant paths ($0.05 \leq p < 0.10$), and solid arrows indicate significant paths ($p < 0.05$). Asterisks indicate statistical significance: * $p < 0.05$, ** $p < 0.01$, and *** $p < 0.001$. Only retained paths are shown. Values beside endogenous variables are R^2. Stress interaction denotes the SSC × SAR interaction.

In *N. tangutorum*, ss had a positive effect on nutrient traits (β = 0.90, $p < 0.001$) and a direct positive effect on biomass (β = 0.54, $p < 0.05$). ADF negatively affected biomass (β = −0.50, $p < 0.05$), whereas SAR positively affected biomass (β = 0.30, $p < 0.01$). SSC exerted a negative effect on nutrient traits (β = −0.18, $p < 0.01$). The model exhibited high explanatory power for nutrient traits and ADF (R^2 = 0.90 and 0.85, respectively) but low explanatory power for biomass (R^2 = 0.08).

In *S. europaea*, SSC and the SSC × SAR interaction were positively associated with biomass (β = 0.44 and 0.21, respectively). SSC had a negative effect on ADF (β = −0.24, $p < 0.05$). The explanatory power was low for nutrient traits and ADF (R^2 = 0.08 and 0.14, respectively) and moderate for biomass (R^2 = 0.28).

3.5. MG-SEM Identified Localized Pathway Differences Within a Common Structural Framework

MG-SEM comparisons revealed that the unconstrained model fit the data significantly better than the equality-constrained model across species ($\Delta\chi^2$ = 95.99, Δdf = 36, $p < 0.001$). Removing weak pathways did not significantly worsen model fit relative to the full unconstrained model ($\Delta\chi^2$ = 9.11, Δdf = 15, $p = 0.871$). AIC decreased from 4390.85 to 4369.96 and BIC from 4763.90 to 4682.84. TLI increased from 0.64 to 0.90, whereas RMSEA decreased from 0.34 to 0.18 and SRMR from 0.09 to 0.08. CFI increased slightly before rounding, but both values round to 0.97.

Within the shared framework, the unconstrained model still outperformed the equality-constrained model ($\Delta\chi^2$ = 88.93, Δdf = 26, $p < 0.001$). Stepwise release of constraints identified three pathways with significant species divergence (FDR-adjusted $p < 0.01$): ss~SSC, biomass~SAR, and nutrient~SSC. For ss~SSC, standardized coefficients were 0.17 in *K. foliatum*, −0.07 in *N. tangutorum*, and 0.42 in *S. europaea*. For biomass~SAR, the corresponding coefficients were 0.004, 0.24, and −0.10, respectively. For nutrient~SSC, the corresponding coefficients were −0.01, −0.14, and 0.02, respectively. Standard errors and 95% confidence intervals for the standardized path coefficients are provided in Table S7. All other pathways did not differ significantly after correction for multiple comparisons. AIC favored the unconstrained model (4369.96 vs. 4406.89), whereas BIC favored the equality-constrained model (4615.48 vs. 4682.84), reflecting a trade-off between fit and parsimony (Table 2).

Table 2. Key heterogeneous paths among species identified by MG-SEM.

Overall model comparison								
Comparison	**$\Delta\chi^2$**	**Δdf**		***p***	**AIC (Free)**	**AIC (Constrained)**	**BIC (Free)**	**BIC (Constrained)**
Free vs. constrained	88.93	26.00		<0.001	4369.97	4406.89	4682.84	4615.48
Key heterogeneous paths								
Path	**$\Delta\chi^2$**	**Δdf**	***p***	**FDR-Adjusted *p***	***K. foliatum* (Std.all)**	***N. tangutorum* (Std.all)**	***S. europaea* (Std.all)**	**Direction**
ss~SSC	18.38	2	<0.001	<0.001	0.17	−0.07	0.42	K:+ | N:− | S:+
Biomass~SAR	18.13	2	<0.001	<0.001	0.004	0.24	−0.10	K:0 | N:+ | S:−
Nutrient~SSC	15.88	2	<0.001	0.002	−0.01	−0.14	0.02	K:0 | N:− | S:0

The upper section compares the unconstrained and cross-species constrained MG-SEMs. The lower section presents heterogeneous pathways identified through nested likelihood-ratio tests after sequentially releasing equality constraints. Standardized coefficients are reported from the unconstrained model. *p* values were adjusted using the Benjamini–Hochberg procedure to control for multiple comparisons.

4. Discussion

Our findings suggest that the three dominant halophytes do not appear to rely on wholly independent regulatory architectures under combined SSC–SAR stress, but differ in specific pathways within a shared stress–trait–performance framework.

4.1. Niche Divergence Along SSC-SAR Gradients Reflects Alternative Adaptive Strategies

The three dominant halophytes differed in niche centroid positions within the SSC–SAR space but showed substantial niche overlap. This indicates that niche differentiation likely reflects species-specific responses to multiple axes of environmental filtering. Halophyte distributions are shaped not only by salinity gradients but also by soil chemical properties, such as pH, sodicity, and ion composition. A single salinity axis is often insufficient to explain habitat differentiation in saline–alkali ecosystems [5,17]. Centroid differences and overlap were evaluated descriptively, without formal tests of centroid separation, null-model comparisons, or spatial adjustment; they therefore do not establish strong niche partitioning.

In this study, SSC and SAR represent two mechanistically distinct dimensions of environmental stress. SSC primarily reflects salt accumulation and associated osmotic stress, whereas SAR is closely related to ionic imbalance and soil chemical and structural changes during salinization and alkalization. These processes impose distinct environmental stresses on plants [18,19].

This is consistent with the adaptive mechanisms of the three species under salinity–alkalinity stress. The distribution of *S. europaea* toward high-SSC environments aligns

with its strong capacity for osmotic adjustment and structural modification. Its adaptation involves not only ion and water regulation but also remodeling of cell-wall nanomechanical properties and lignin composition, which may help contribute to maintaining tissue hydration and structural stability [20]. In contrast, *K. foliatum* sustains photosynthetic function and antioxidant homeostasis under salinity–alkalinity stress by modulating photosynthetic pigments, Rubisco activity, and SOD activity [21]. This strategy aligns with its relatively intermediate position in the SSC-SAR space and the absence of strong directional trait coordination. For *N. tangutorum*, NtSOS2 has been shown to enhance salt tolerance by regulating the expression of ion transport-related genes, improving antioxidant capacity, and maintaining root growth and biomass under saline conditions [22]. The reported ion homeostasis-antioxidant regulatory mechanism may provide a plausible explanation for the tendency of *N. tangutorum* to occupy high-SAR regions of the niche space observed in this study.

4.2. Trait Coordination Differs Among the Three Dominant Halophytes

Interspecific differences among the three dominant halophytes were primarily reflected in the differentiation of coordination mechanisms among osmotic regulation, nutrient maintenance, structural investment, and biomass formation. Across all three species, ss showed stable positive associations with nutrient traits, indicating a conserved coupling between osmotic adjustment and nutrient maintenance. This pattern is consistent with the coordinated regulation of osmotic adjustment, ionic homeostasis, and nutrient balance that underpins plant adaptation to saline–alkali environments [23,24].

The major axis of interspecific divergence was associated with the relationship between structural investment (ADF) and biomass accumulation. In *N. tangutorum*, ADF exerted a significant negative effect on biomass. This suggests that increased structural investment is associated with reduced growth allocation. This pattern reflects a resource-conservative strategy, where investment in cell-wall reinforcement and tissue maintenance occurs at the expense of biomass accumulation. Similar trade-offs have been reported in salt-marsh plants, in which stress gradients reshape biomass allocation through trait-mediated mechanisms [25]. At the same time, increased structural investment is often associated with reduced fitness outcomes [26]. By contrast, the ADF–biomass relationship was weak or non-significant in *K. foliatum* and *S. europaea*, suggesting that structural investment did not impose a consistent growth cost in these species. This indicates that the functional role of ADF is context-dependent, varying with how each species balances structural maintenance against growth allocation under combined salinity–alkalinity stress.

In addition, species differed in how SSC and SAR were linked to biomass formation. In *K. foliatum* and *S. europaea*, biomass increased primarily along the SSC gradient, whereas *N. tangutorum* showed weak sensitivity to SSC but a stronger positive response to SAR, as also supported by SEM results. These findings suggest that biomass is associated with different dominant stress axes among species. However, the biomass R^2 for *N. tangutorum* was only 0.08, leaving approximately 92% of the observed variation unexplained. The detected associations therefore provide only a partial account of biomass variation and do not establish structural investment or SAR as its predominant determinants. Although both sites were sampled during the peak-biomass period, differences in growing-season length and plant life history may contribute to site-dependent biomass–environment relationships. Chaka's shorter growing season relative to Dingbian may influence the time available for biomass accumulation in the annual herb *S. europaea*. In contrast, the measured biomass of the perennial subshrub *K. foliatum* and shrub *N. tangutorum* included woody tissues retained from previous years and therefore reflected growth accumulated across multiple growing seasons. These contrasting temporal scales of biomass accumu-

lation may contribute to species-specific associations between standing biomass and soil salinity–alkalinity conditions.

Overall, the three species exhibited distinct modes of trait coordination under SSC-SAR stress. *S. europaea* relied more strongly on coordination between osmotic regulation and nutrient maintenance. In *N. tangutorum*, the negative ADF–biomass association suggested a possible trade-off between structural investment and biomass accumulation, although this interpretation remains tentative given the low R^2 for biomass (0.08). *K. foliatum* displayed relatively balanced trait coordination. These results indicate that interspecific differentiation primarily arises from the reorganization of trait coordination networks rather than from shifts in individual trait magnitudes.

4.3. Species Divergence Is Superimposed on a Shared Mechanistic Framework

MG-SEM results suggested that the three dominant halophytes exhibited species-specific associations within a broadly shared stress–trait–performance framework. Removing weak pathways did not significantly worsen model fit relative to the full unconstrained model. The models linked SSC and SAR to biomass through associations involving osmotic, nutrient, and structural traits. Thus, adaptive divergence among the three species appears to arise not from a complete reorganization of the underlying regulatory architecture, but from differential regulation of specific components operating under shared physiological constraints. This interpretation is consistent with previous studies, which demonstrated that plant responses to multiple abiotic stresses are governed by coordinated physiological and molecular networks, involving both shared and stress-specific adjustments. Diversified adaptation strategies primarily result from the modulation and optimization of physiological processes [27,28].

However, support for interspecific differentiation was not uniform across model-selection criteria. AIC favored the unconstrained model, whereas BIC favored the more parsimonious equality-constrained model (Table 2). This contrast indicates that the improvement in fit was sufficient to offset the additional parameters under AIC, but not under BIC's stronger complexity penalty. Thus, the pathway-specific differences should not be taken as definitive evidence that broadly different parameterizations are required for the three species.

Path-level comparisons identified significant interspecific differences in three of the 13 tested relationships: ss~SSC, biomass~SAR, and nutrient~SSC. The remaining pathways did not differ significantly after correction for multiple comparisons, although this does not establish that their coefficients were identical across species. The SSC–ss association was strongest in *S. europaea* ($\beta = 0.42$), while the positive SAR–biomass association was strongest in *N. tangutorum* ($\beta = 0.24$). However, the standardized SSC–nutrient coefficients were relatively small ($\beta = -0.14$ to 0.02), despite significant interspecific differences. These findings support localized differences in particular associations within the shared framework, rather than providing evidence for a wholesale reconfiguration of the underlying network architecture. This pattern is consistent with t the role of trait coordination and trade-offs in shaping interspecific differentiation [29].

This "localized pathway differentiation within a shared framework" pattern may arise from the coupling between shared functional requirements under salinity–alkalinity stress and species-specific resource allocation strategies. Plant responses to salt accumulation and sodification involve osmotic regulation, nutrient maintenance, structural stability, and growth allocation. Within this framework, the relative importance of these processes may vary among species. The stronger SSC–ss association in *S. europaea* may reflect osmotic adjustment, complementing previously reported cell-wall remodeling under salinity [20]. The positive SAR–biomass association in *N. tangutorum* may involve ion regulation, a

possibility informed by NtSOS2-mediated salt tolerance in transgenic *Arabidopsis* [22]. Its weak negative SSC–nutrient association may indicate modest constraints on nutrient maintenance. These interpretations require direct validation, and salt-tolerance evidence does not establish high SAR tolerance.

Taken together, the results suggest localized interspecific differences within a shared stress–trait–performance framework. The contrasting AIC and BIC preferences nevertheless warrant caution in interpreting these differences as evidence of broadly divergent adaptive strategies.

4.4. Implications for Halophyte Coexistence and Saline–Alkali Land Restoration

Dominant halophytes in saline–alkali habitats occupy distinct positions in the SSC-SAR space through differentiated trait coordination strategies. Therefore, species coexistence is shaped not only by overall stress intensity but also by how soil salinity and sodicity jointly shape environmental heterogeneity and promote functional differentiation. From a practical perspective, this implies that restoration strategies for saline–alkali land should move beyond single-index salinity tolerance and instead account for multidimensional environmental conditions. Different species are preferentially adapted to distinct stress axes. Some are better adapted to increasing SSC, while others respond more strongly to varying SAR. Therefore, species configuration should explicitly match local SSC-SAR profiles with species-specific functional strategies.

Several limitations should be noted. First, this study was based on field observations and trait associations. Therefore, it revealed mechanistic patterns but did not provide direct experimental validation. Future research should incorporate transplantation experiments or long-term monitoring to further verify the findings of this study. Additionally, neighboring sampling points along transects may share similar environmental conditions and therefore may not be fully independent. The SEM and MG-SEM analyses in this study did not account for this potential spatial dependence, which may affect standard error estimates and the interpretation of path significance. Sampling was also limited to July–August 2021. Repeated surveys across seasons and water-availability conditions would help assess whether the observed relationships persist as soil salt concentrations and distribution change. Second, SSC and SAR captured two key dimensions of saline–alkali stress. However, other factors, such as soil pH, ion composition, soil moisture, microtopography, and background nutrient availability, may also influence plant performance. Finally, physiological processes were inferred from functional traits rather than measured directly; measurements of ion fluxes and plant water potential would help test the proposed mechanisms.

5. Conclusions

This study conducted functional trait analyses of three dominant halophytes from two representative saline–alkali habitats in northwestern China. The three species occupied different positions within broadly overlapping niches in the two-dimensional SSC–SAR stress space and exhibited distinct patterns of trait coordination involving osmotic regulation, nutrient maintenance, structural investment, and biomass accumulation. This differentiation appears to involve variation in specific pathways within a shared stress–trait–performance framework. However, the low biomass R^2 for N. tangutorum (0.08) limits inference about its overall growth strategy. The findings of this study provide a trait-based perspective on the differentiation and coexistence of dominant species in saline–alkali ecosystems. From an applied perspective, restoration planning may benefit from considering both SSC and SAR alongside species-specific trait patterns, rather than relying on a single salinity indicator.

Supplementary Materials: The following supporting information can be downloaded at https://www.mdpi.com/article/10.3390/agronomy16212104/s1: Table S1: Sampling effort and availability

of core plant trait measurements by species and site; Table S2: Summary of GAM results for two-dimensional niche response surfaces of the three dominant halophytes along SSC and SAR gradients; Table S3: Species-specific 1D threshold positions and effect sizes for key traits along SSC and SAR gradients; Table S4: Effect sizes and uncertainty in expected trait responses across the original thresholds; Table S5: Environment-adjusted EBICglasso partial-correlation networks for five core traits (γ = 0.20); Table S6: Sensitivity summary of species-specific functional trait networks under a weaker EBICglasso penalty (γ = 0.10); Table S7: Standardized coefficients and uncertainty for the key MG-SEM paths; Figure S1: Species-specific biomass regression models at the Chaka and Dingbian sites; Figure S2: Species-specific functional trait networks of three dominant halophytes.

Author Contributions: Conceptualization, S.M., G.L. and S.X.; methodology, S.M., Z.Y. and Y.W.; validation, Z.Y.; formal analysis, S.M. and F.Z.; investigation, S.M., Y.W., M.L. and H.X.; resources, Z.Y. and S.X.; data curation, S.M.; writing—original draft preparation, S.M.; writing—review and editing, S.M., Z.Y., F.Z. and S.X.; visualization, S.M.; supervision, G.L.; project administration, S.X.; funding acquisition, S.X. All authors have read and agreed to the published version of the manuscript.

Funding: This study was supported by the Regional Innovation and Development Joint Fund of the National Natural Science Foundation of China (No. U24A20642).

Data Availability Statement: The data supporting the findings of this study are available from the corresponding author upon reasonable request.

Acknowledgments: The authors gratefully acknowledge the technical assistance provided during field sampling and laboratory analyses, as well as the institutional support for this research.

Conflicts of Interest: Author Zengbi Yue was employed by the company Power China Northwest Engineering Corporation Limited. The remaining authors declare that the research was conducted in the absence of any commercial or financial relationships that could be construed as a potential conflict of interest.

References

1. Jat Baloch, M.Y.; Zhang, W.; Sultana, T.; Akram, M.; Shoumik, B.A.A.; Khan, M.Z.; Farooq, M.A. Utilization of sewage sludge to manage saline–alkali soil and increase crop production: Is it safe or not? *Environ. Technol. Innov.* **2023**, *32*, 103266. [CrossRef]
2. Liang, B.; Wei, J.; Gao, Y.; Ma, Z.; Xue, X. A review of classification, causes, and amelioration of global salt-affected soil based on the meta-analysis. *Land Degrad. Dev.* **2025**, *36*, 5485–5504. [CrossRef]
3. Tang, H.; Du, L.; Xia, C.; Luo, J. Bridging gaps and seeding futures: A synthesis of soil salinization and the role of plant-soil interactions under climate change. *iScience* **2024**, *27*, 110804. [CrossRef] [PubMed]
4. Stavi, I.; Thevs, N.; Priori, S. Soil salinity and sodicity in drylands: A review of causes, effects, monitoring, and restoration measures. *Front. Environ. Sci.* **2021**, *9*, 712831. [CrossRef]
5. Pätsch, R.; Midolo, G.; Dítě, Z.; Dítě, D.; Wagner, V.; Pavonič, M.; Danihelka, J.; Preislerová, Z.; Ćuk, M.; Stroh, H.G.; et al. Beyond salinity: Plants show divergent responses to soil ion composition. *Glob. Ecol. Biogeogr.* **2024**, *33*, e13821. [CrossRef]
6. Rao, Y.; Peng, T.; Xue, S. Mechanisms of plant saline-alkaline tolerance. *J. Plant Physiol.* **2023**, *281*, 153916. [CrossRef] [PubMed]
7. Global Map of Salt-Affected Soils (GSASmap) | Global Soil Partnership | FAO. Available online: http://www.fao.org/global-soil-partnership/soil-data/global-map-of-salt-affected-soils-gsasmap/en (accessed on 26 September 2026).
8. Barton, K.E. The ontogenetic dimension of plant functional ecology. *Funct. Ecol.* **2024**, *38*, 98–113. [CrossRef]
9. Li, J.; Prentice, I.C. Global patterns of plant functional traits and their relationships to climate. *Commun. Biol.* **2024**, *7*, 1136. [CrossRef] [PubMed]
10. Díaz, S. Plant functional traits and the entangled phenotype. *Funct. Ecol.* **2025**, *39*, 1144–1159. [CrossRef]
11. Gomarasca, U.; Migliavacca, M.; Kattge, J.; Nelson, J.A.; Niinemets, Ü.; Wirth, C.; Cescatti, A.; Bahn, M.; Nair, R.; Acosta, A.T.R.; et al. Leaf-level coordination principles propagate to the ecosystem scale. *Nat. Commun.* **2023**, *14*, 3948. [CrossRef] [PubMed]
12. Chen, Y.; Hautier, Y.; Kowalchuk, G.A.; Barry, K.E. 'Slow-fast' plant trait spectra are associated with ecological niches across global climatic gradients. *Glob. Ecol. Biogeogr.* **2025**, *34*, e70115. [CrossRef]
13. Zhang, C.; Gu, R.; Lin, L.; Russo, S.E. Functional traits and ecological niches as correlates of the interspecific growth–mortality trade-off among seedlings of 14 tropical tree species. *Funct. Ecol.* **2024**, *38*, 1888–1901. [CrossRef]
14. Pérez-Ramos, I.M.; Matías, L.; Gómez-Aparicio, L.; Godoy, Ó. Functional traits and phenotypic plasticity modulate species coexistence across contrasting climatic conditions. *Nat. Commun.* **2019**, *10*, 2555. [CrossRef] [PubMed]

15. Karim, M.R.; Karmaker, N.; Biswas, S.R.; Saimun, M.S.R.; Mukul, S.A.; Khatun, T.; Sultana, F.; Srivastava, S.K.; Arfin-Khan, M.A.S. Trait-based evidence of salinity-induced functional diversity loss in mangroves: Implications for ecosystem resilience. *Ecol. Appl.* **2026**, *36*, e70191. [CrossRef] [PubMed]
16. Yan, P.; He, N.; Yu, K.; Xu, L.; Van Meerbeek, K. Integrating multiple plant functional traits to predict ecosystem productivity. *Commun. Biol.* **2023**, *6*, 239. [CrossRef] [PubMed]
17. Kramer, I.; Mau, Y. Review: Modeling the effects of salinity and sodicity in agricultural systems. *Water Resour. Res.* **2023**, *59*, e2023WR034750. [CrossRef]
18. Fang, S.; Hou, X.; Liang, X. Response mechanisms of plants under saline-alkali stress. *Front. Plant Sci.* **2021**, *12*, 667458. [CrossRef] [PubMed]
19. Lin, J.; Shao, S.; Wang, Y.; Qi, M.; Lin, L.; Wang, Y.; Yan, X. Germination responses of the halophyte chloris virgata to temperature and reduced water potential caused by salinity, alkalinity and drought stress. *Grass Forage Sci.* **2016**, *71*, 507–514. [CrossRef]
20. Cárdenas Pérez, S.; Strzelecki, J.; Piernik, A.; Rajabi Dehnavi, A.; Trzeciak, P.; Puchałka, R.; Mierek-Adamska, A.; Chanona Pérez, J.; Kačík, F.; Račko, V.; et al. Salinity-driven changes in *salicornia* cell wall nanomechanics and lignin composition. *Environ. Exp. Bot.* **2024**, *218*, 105606. [CrossRef]
21. Gong, D.H.; Wang, G.Z.; Si, W.T.; Zhou, Y.; Liu, Z.; Jia, J. Effects of salt stress on photosynthetic pigments and activity of ribulose-1,5-bisphosphate carboxylase/oxygenase in kalidium foliatum. *Russ. J. Plant Physiol.* **2018**, *65*, 98–103. [CrossRef]
22. Zhu, L.; Li, M.; Huo, J.; Lian, Z.; Liu, Y.; Lu, L.; Lu, Y.; Hao, Z.; Shi, J.; Cheng, T.; et al. Overexpression of ntsos2 from halophyte plant n. tangutorum enhances tolerance to salt stress in arabidopsis. *Front. Plant Sci.* **2021**, *12*, 716855. [CrossRef] [PubMed]
23. Pérez-López, A.V.; Lim, S.D.; Cushman, J.C. Humboldt review: Tissue succulence in plants: Carrying water for climate change. *J. Plant Physiol.* **2023**, *289*, 154081. [CrossRef] [PubMed]
24. Rahman, M.M.; Mostofa, M.G.; Keya, S.S.; Siddiqui, M.N.; Ansary, M.M.U.; Das, A.K.; Rahman, M.A.; Tran, L.S.-P. Adaptive mechanisms of halophytes and their potential in improving salinity tolerance in plants. *Int. J. Mol. Sci.* **2021**, *22*, 10733. [CrossRef] [PubMed]
25. De Battisti, D.; Fowler, M.S.; Jenkins, S.R.; Skov, M.W.; Bouma, T.J.; Neyland, P.J.; Griffin, J.N. Multiple trait dimensions mediate stress gradient effects on plant biomass allocation, with implications for coastal ecosystem services. *J. Ecol.* **2020**, *108*, 1227–1240. [CrossRef]
26. VanWallendael, A.; Soltani, A.; Emery, N.C.; Peixoto, M.M.; Olsen, J.; Lowry, D.B. A molecular view of plant local adaptation: Incorporating stress-response networks. *Annu. Rev. Plant Biol.* **2019**, *70*, 559–583. [CrossRef] [PubMed]
27. Busoms, S.; Fischer, S.; Yant, L. Chasing the mechanisms of ecologically adaptive salinity tolerance. *Plant Commun.* **2023**, *4*, 100571. [CrossRef] [PubMed]
28. Jiang, Z.; van Zanten, M.; Sasidharan, R. Mechanisms of plant acclimation to multiple abiotic stresses. *Commun. Biol.* **2025**, *8*, 655. [CrossRef] [PubMed]
29. Muñoz-Gálvez, F.J.; Querejeta, J.I.; Moreno-Gutiérrez, C.; Ren, W.; de la Riva, E.G.; Prieto, I. Trait coordination and trade-offs constrain the diversity of water use strategies in mediterranean woody plants. *Nat. Commun.* **2025**, *16*, 4103. [CrossRef] [PubMed]

Disclaimer/Publisher's Note: The statements, opinions and data contained in all publications are solely those of the individual author(s) and contributor(s) and not of MDPI and/or the editor(s). MDPI and/or the editor(s) disclaim responsibility for any injury to people or property resulting from any ideas, methods, instructions or products referred to in the content.